Journal of Molecular Spectroscopy 348 (2018) 79–86

Contents lists available at ScienceDirect

Journal of Molecular Spectroscopy

journal homepage: www.elsevier.com/locate/jms

The $2v_6/v_2 + v_3/v_3 + v_5$ band system of CH_3Br revisited: Modeling anharmonic and Coriolis interactions in a three-level system near 2000 cm^{-1}

Adina Ceausu-Velcescu [a,*], Fridolin Kwabia Tchana [b], Xavier Landsheere [b]

[a] Univ. Perpignan Via Domitia, Laboratoire de Mathématiques et Physique, EA 4217, F-66860 Perpignan, France
[b] Laboratoire Interuniversitaire des Systèmes Atmosphériques (LISA), UMR CNRS 7583, Université Paris Est Créteil and Paris Diderot, Institut Pierre Simon Laplace, 61 Avenue du Général de Gaulle, 94010 Créteil Cedex, France

ARTICLE INFO

Article history:
Received 18 April 2017
Accepted 14 May 2017
Available online 20 May 2017

Keywords:
Methyl bromide
Anharmonic
Coriolis and α-resonance interactions
Combination bands
High resolution
IR absorption

ABSTRACT

The $2v_6$ (A_1 + E)/$v_2 + v_3$ (A_1)/$v_3 + v_5$ (E) band system of CH_3Br, near 2000 cm^{-1}, has been studied, for both ^{79}Br and ^{81}Br isotopologues, using Fourier transform infrared spectroscopy, with a resolution of 0.003 cm^{-1}. This band system, revealing anharmonic ($\Delta k = \Delta l = 0$) and Coriolis ($\Delta k = \Delta l = \pm 1$) interactions, has been analyzed through a least-squares fit of more than 3000 transitions, for each isotopologue. More than 600 transitions belonging to the very weak $v_3 + v_5$ combination band were assigned for the first time, for both $CH_3{}^{79}Br$ and $CH_3{}^{81}Br$ isotopologues. Assignments of the weak $2v_6^0$ parallel band, which is Fermi-interacting with $v_2 + v_3$, were also considerably extended with respect to a previous high-resolution study (Najib et al., 1985), thanks to a more accurate knowledge of the Fermi coupling parameters and of the relative positions of the interacting levels.

The least-squares fits provided quantitative reproduction of all data belonging to the four above mentioned bands. Moreover, the Coriolis coupling parameters obtained for the $v_2 + v_3/v_3 + v_5$ interacting bands show a remarkable consistency with those obtained for the v_2/v_5 'fundamental' system (Kwabia Tchana et al., 2004).

1. Introduction

Methyl bromide (CH_3Br) is a stratospheric ozone depleting substance that, unlike many other ozone-depleting compounds, has both natural and anthropogenic sources. However, the atmospheric CH_3Br burden has declined in recent years, in response to the phase out of agricultural and structural fumigation consumption, under the amendments to the Montreal Protocol [1]. We have to notice in passing that sulfuryl difluoride (SO_2F_2) is used increasingly as a fumigant to replace methyl bromide for controlled uses because it does not directly cause ozone depletion, but it has a calculated direct, 100-year Global Warming Potential (GWP_{100}) of 4740 [2].

A recent study [3] estimates that methyl bromide is actually present in the atmosphere at a mole fraction, or volume mixing ratio, of around 7 ppt (1 part per trillion (ppt) = 10^{-12} mol of gas per mole of air). A 20% reduction of the atmospheric concentration of this gas between 1995 and 2012, due to the phase out of anthropogenic emissions (begun in 2005), can thus be observed. Nevertheless, accurate monitoring methyl bromide in our environment is still of interest, for both environmental and health concerns.

In order to achieve a quantitative retrieval of atmospheric profiles, precise line positions, as well as air-broadening coefficients, are required. Spectroscopic databases, such as GEISA [4] or HITRAN [5], comprise however, for methyl bromide, a relatively narrow spectral region, from 700 to 1700 cm^{-1}. Overtone and combination bands are thus not included so far, even though their intensity could be quite important.

The high-resolution spectroscopic analyses of the overtone and combination bands of a molecule are of crucial importance for the accurate modeling of its absorption in the mid and near infrared regions. However, such analyses are generally difficult to undertake, often because of the low intensity of the studied bands, but also of the complexity of the vibrational pattern. Indeed, such overtone and combination vibrational states are rarely isolated, being more often involved in vibrational polyads. This explains why, for instance, only a few studies are dealing with overtone or

* Corresponding author at: Université de Perpignan Via Domitia, Laboratoire de Mathématiques et Physique, 52 Avenue Paul Alduy, F-66860 Perpignan, France.
E-mail address: adina@univ-perp.fr (A. Ceausu-Velcescu).

http://dx.doi.org/10.1016/j.jms.2017.05.010
0022-2852/

Table 1
Summary of experimental conditions used to record the Fourier transform infrared (1550–2250 cm^{-1}) spectra of CH_3Br.

Spectrum	Source	Detector	Beam splitter	Resolution (cm^{-1})	Aperture diameter (mm)	Cell optical path length (m)	Sample pressure (Pa)	Temperature (K)	Measuring time (h)	No. of scans	Calibration gas
I	Globar	InSb	KBr/Ge	0.003	1.15	32.05 (10)	336.4 (4)	297 ± 1	5.4	162	CO_2 and H_2O
II	Globar	MCT	KBr/Ge	0.003	1	41.65 (12)	467.2 (2.4)	297 ± 1	43	1290	CO_2 and H_2O

combination bands of CH_3Br, most of them performed with medium resolution, more than thirty years ago [6–9].

The infrared spectrum of CH_3Br shows a strong parallel band centered at 1912 cm^{-1}; it is the $\nu_2 + \nu_3$ combination band, detected early in 1965 by Morino et al. [7], in a low-resolution (0.6 cm^{-1}) spectrum. A first high-resolution (0.005 cm^{-1}) study of this band, together with the, less intense, $2\nu_6^{\mp 2}$ overtone band, has been performed by Najib et al. [8]. The latter authors assigned a total of 750 rovibrational transitions of the $\nu_2 + \nu_3$ band, 750 transitions of the $2\nu_6^{\mp 2}$ perpendicular overtone band, and four *K*-subbands of the $2\nu_6^0$ parallel overtone band. In their study, no lines were assigned for the, very weak, $\nu_3 + \nu_5$ combination band, which interacts through an *x*, *y*-Coriolis resonance with $\nu_2 + \nu_3$. The present study considerably extends the assignments in the $\nu_2 + \nu_3$, $2\nu_6^{\mp 2}$ and $2\nu_6^0$ bands, for both $CH_3{}^{79}Br$ and $CH_3{}^{81}Br$ isotopologues. Particularly, several *K*-series of lines of the, otherwise very weak, $2\nu_6^0$ parallel band, enhanced by intensity stealing from the $\nu_2 + \nu_3$ band, could be followed beyond the Fermi crossings. Moreover, several *K*-subbands of the very weak $\nu_3 + \nu_5$ perpendicular band could be unambiguously assigned and checked by lower state combination differences (LSCD). In this way, the band center of the above mentioned combination band could be accurately obtained, together with the Coriolis coupling parameter with $\nu_2 + \nu_3$, for both isotopologues. The interaction picture within the $2\nu_6/\nu_2 + \nu_3/\nu_3 + \nu_5$ polyad is now completely understood.

2. Experimental details

The high-resolution absorption spectra of CH_3Br molecule were recorded using the Bruker IFS 125HR Fourier transform spectrometer (an upgraded version of the IFS 120HR) at LISA in Créteil. The spectrometer was equipped with a Globar source, a KBr/Ge beamsplitter and a liquid nitrogen cooled HgCdTe (MCT) or Indium Antimonide (InSb) detector was used. The Fourier transform spectrometer (FTS) was evacuated down to 6.7 Pa pressure in order to minimize residual H_2O and CO_2 absorption in the spectrum. The aperture diameter (1 or 1.15 mm) of the spectrometer was set to maximize the intensity of IR radiation falling onto the detector without saturation or loss of spectral resolution. Spectrum was recorded with a 40 kHz scanner frequency and a maximum optical path difference (d_{MOPD}) of 300 cm. According to the Bruker definition (Resolution = $0.9/d_{MOPD}$), this corresponds to a resolution of 0.003 cm^{-1}.

The White-type multipass absorption cell, made of Pyrex glass and equipped with CsBr windows, was connected to the FTS with a dedicated optical interface (six mirrors) inside the sample chamber of the FTS. Its base length is 0.80 m, and, for the experiment described here, an optical path of 32.05 (10) or 41.65 (12) m was used. This value takes into account the distance between the surface of the field mirror and the windows of the cell (2 × 2.45 cm).

The CH_3Br sample (99% stated purity with bromine at natural abundance i.e., 50.54% ^{79}Br and 49.46% ^{81}Br) was purchased from Sigma Aldrich and was used without further purification. The following procedure was used for measurements: first a background spectrum was collected while the cell was being continuously evacuated; next the infrared gas cell was treated with CH_3Br several times, until no proton exchange with the surface could be detected and, for the final measurements, two sample pressures were used (Table 1).

The sample pressure in the cell was measured using a calibrated MKS Baratron gauge model 627 D (1333.22 Pa full scale) with an accuracy reading of 0.12%, according to the manufacturer. To estimate the uncertainty of the sample pressure, we add the uncertainty arising from the small variation of the pressure during the recording (∼0.35%) and the accuracy of the gauge; this leads to an estimation of 0.5% uncertainty on the pressure. The spectra were recorded at a stabilized room temperature of 297 ± 1 K.

The spectra were ratioed against a single channel background spectrum of the empty cell which was recorded at a resolution of 0.2 cm^{-1} in order to ensure the best possible signal-to-noise in the ratioed spectra. For the Fourier transform, a Mertz-phase correction, 1 cm^{-1} phase resolution, a zero-filling factor of 2 and a boxcar apodization function were applied to the averaged interferograms. The FTS instrumental parameters and details of pressure and number of scans are summarised in Table 1.

The spectra were calibrated with residual CO_2 and H_2O lines observed in the spectra with their wavenumbers taken from HITRAN [5]. The resulting accuracy is ±0.0003 cm^{-1} (RMS) for well isolated lines.

3. Description of the spectra and assignments

3.1. The $\nu_2 + \nu_3$ and $2\nu_6^{\mp 2}$ bands

The most intense $\nu_2 + \nu_3$ band and the $2\nu_6^{\mp 2}$ perpendicular overtone band have been extensively described in Ref. [8]. Their main characteristics will therefore not be recalled here. We will only say that the $2\nu_6^{\mp 2}$ band looks almost unperturbed, which might explain its separate treatment in Ref. [8]. However, two 'local' perturbations affecting this band have to be noticed. First, the $^PX_3$ ($X = P, Q, R$) lines appear as doublets which become resolved for $J' \geq 31$ (Fig. 1). This splitting, increasing with *J*, reaches $\sim 8.8 \times 10^{-3}$ cm^{-1} for $J' = 37$ and could be correctly reproduced only after having introduced a ($\Delta k = \Delta l = \pm 4$) intra-vibrational resonance in the theoretical model. The second perturbation is due to a ($\Delta k = \pm 1$, $\Delta l = \mp 2$) interaction with $\nu_2 + \nu_3$, already pointed out in Ref. [8]. As this perturbation mainly affects the $^PX_1$ ($X = P, Q, R$) series of the $2\nu_6^{\mp 2}$ band, the corresponding lines were simply excluded from the least-squares fit of Ref. [8]. This was no more the case of the present contribution, where a global least-squares calculation has been performed on the whole set of assigned wavenumbers.

3.2. The $\nu_3 + \nu_5$ combination band

The main achievement of the present study is the unambiguous assignment of the $\nu_3 + \nu_5$ combination band, allowed by the identification and assignment of several *Q*-branches, between 1980 and 2100 cm^{-1}. These *Q*-branches, which are however very weak ($T \sim 0.95$, see Fig. 2), are regularly spaced by about 11.8 cm^{-1}, which corresponds to the value of $2(A - B - A\zeta)$ and show a clear

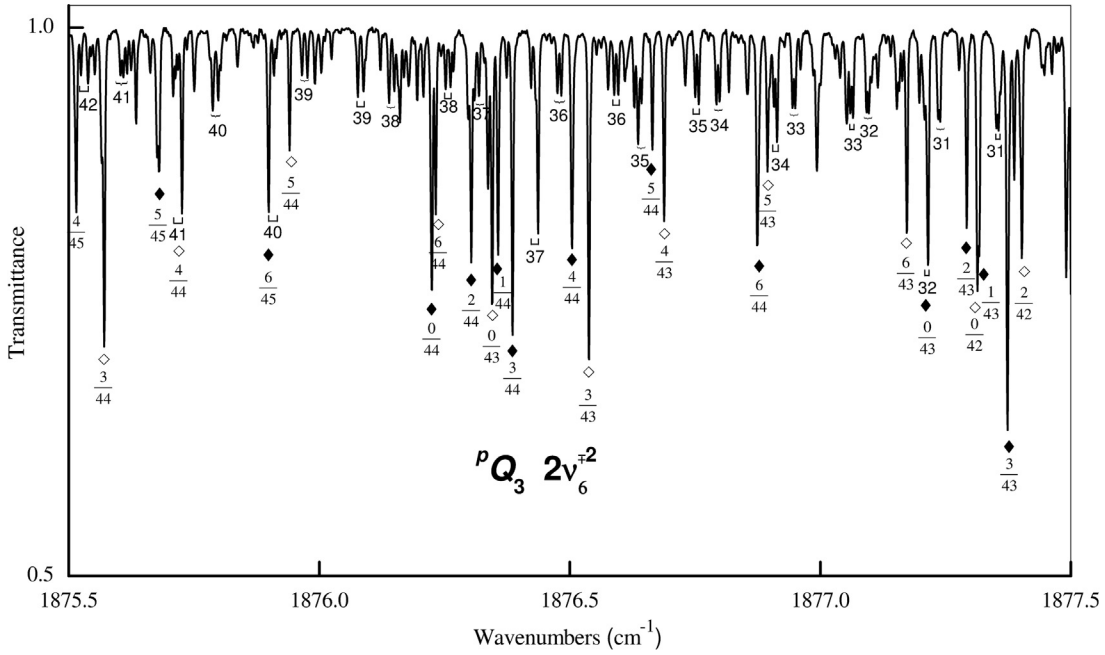

Fig. 1. Detail of the infrared spectrum of CH_3Br, showing the $^pQ_3$ branch of the $2\nu_6^{\mp 2}$ band. The J-lines, the assignments of which are indicated, appear as doublets, resolved for $J \geq 31$ (⌴ for $CH_3{}^{79}Br$ and ⌣ for $CH_3{}^{81}Br$). The most intense lines, for which some K/J values are indicated (◆ for $CH_3{}^{79}Br$ and ◇ for $CH_3{}^{81}Br$), are ^qP_k lines of the $\nu_2 + \nu_3$ band. Experimental conditions: pressure 336.4 Pa, path length 32.05 m, resolution $(0.9/d_{MOPD})$ 0.003 cm^{-1}.

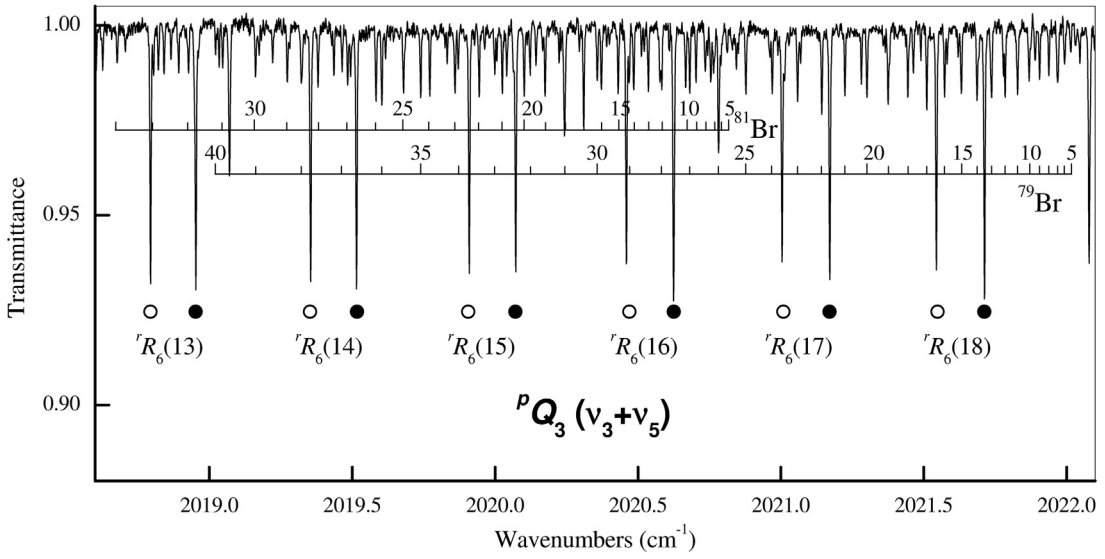

Fig. 2. Detail of the infrared spectrum of CH_3Br, showing the $^pQ_3$ branch of the $\nu_3 + \nu_5$ band, with some J-assignments indicated. The most intense, regularly spaced lines belong to the $2\nu_6^{\mp 2}$ band (● for $CH_3{}^{79}Br$ and ○ for $CH_3{}^{81}Br$). Experimental conditions as those for Fig. 1.

intensity alternation due to nuclear spin statistics. The $^rQ_0$ branch, starting near 2058 cm^{-1} for $CH_3{}^{79}Br$ and near 2057 cm^{-1} for $CH_3^{81}Br$ (Fig. 3), shows almost the same spacing between J-lines as the neighboring $^pQ_1$ and $^rQ_1$ branches, which suggests that the q_{22} l-resonance parameter is small. A careful inspection shows that the ($kl = +1$) sublevel of $v_3 = v_5 = 1$ has however a large asymmetric A_+/A_- splitting,[1] with the A_- component which is almost unaffected, whereas the A_+ component is pushed up by about 1 cm^{-1}, for J=31. This effect, due to the x, y-Coriolis interaction with ($v_2 = v_3 = 1$), was observed already in the late fifties by Garing et al. [10], who called it "giant l-type doubling". Indeed, contrarily to the "normal" l-type doubling, which is symmetric and is due to a second-order interaction, the giant l-type doubling is a first-order effect.

Once the J-assignments performed in each Q-branch[2], the assignments by lower state combination differences (LSCD) of the corresponding P ($\Delta J = -1$) and R ($\Delta J = +1$) branches is quite straightforward. The interactive LSCD checking method [11] allowed us to assign more than 600 rovibrational wavenumbers of the $\nu_3 + \nu_5$ band, with $-9 \leq K'' \Delta K \leq +6$ and $J_{max} = 48$, for both isotopologues.

[1] The A_+ sublevel is of A_1 symmetry for J even and of A_2 symmetry for J odd; the reverse occurs for the A_- sublevel.

[2] The transition wavenumbers of a given Q-branch depend on $J(J+1)$ and are hence quite sensitive to the J assignments. A least-squares fit of the Q-branch wavenumbers as a function of $J(J+1)$ gives a standard deviation reaching a minimum for the correct J values.

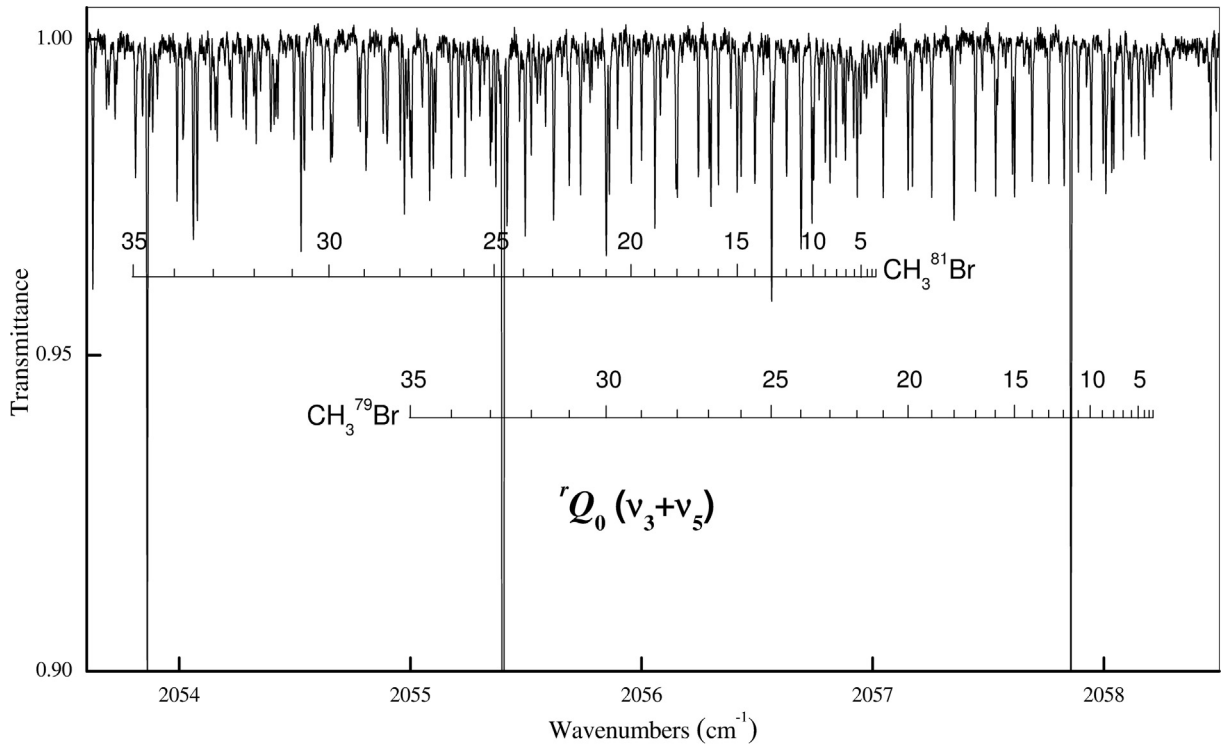

Fig. 3. Detail of the infrared spectrum of CH_3Br, showing the $^rQ_0$ branch of the $\nu_3 + \nu_5$ band, with some *J*-assignments indicated. Experimental conditions as those for Fig. 1.

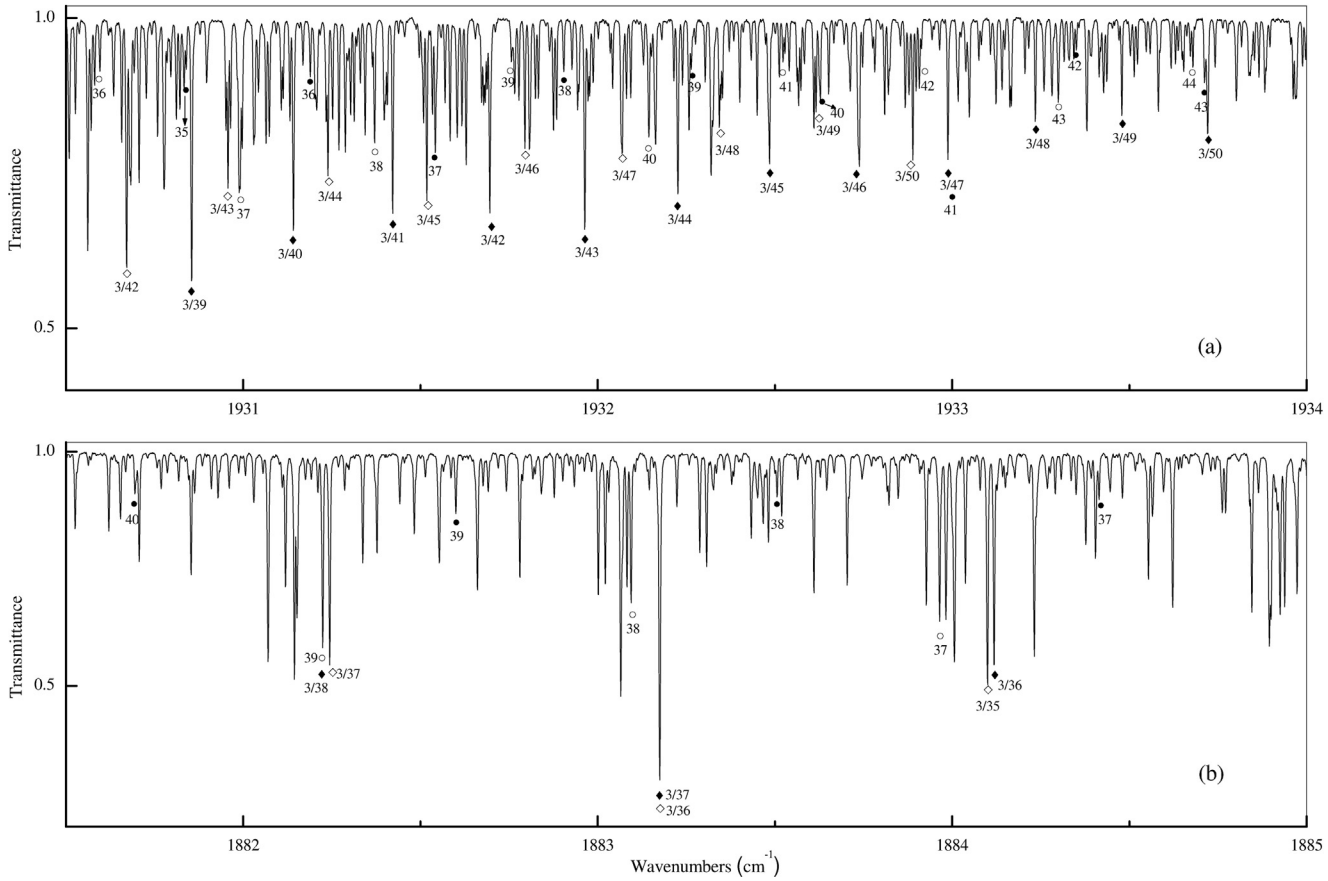

Fig. 4. (a) Detail of the infrared spectrum of CH_3Br, showing several $^qR_9$ lines of the $2\nu_6^0$ band (● for $CH_3{}^{79}Br$ and ○ for $CH_3{}^{81}Br$), enhanced by intensity stealing from $\nu_2 + \nu_3$. Some *K*|*J* assignments in the $^qR_3$ series of the $\nu_2 + \nu_3$ band, for $CH_3{}^{79}Br$ (◆) and $CH_3{}^{81}Br$ (◇), are equally indicated. (b) The corresponding $^qP_9$ lines of the same band, found by LSCD. Some *K*|*J* assignments in the $^qP_3$ series of the $\nu_2 + \nu_3$ band, for $CH_3{}^{79}Br$ (◆) and $CH_3{}^{81}Br$ (◇), are equally indicated. Experimental conditions as those for Fig. 1.

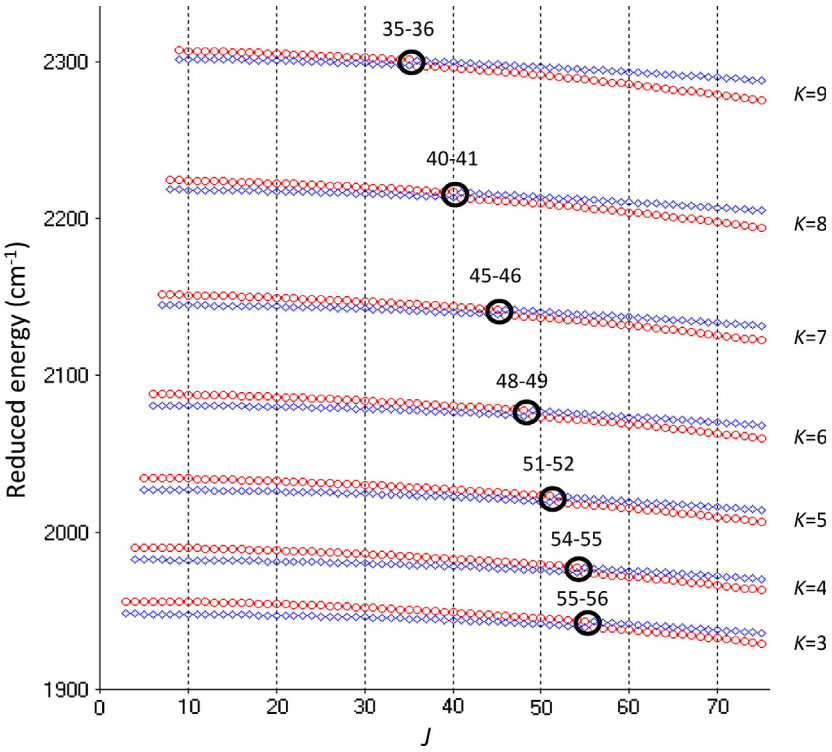

Fig. 5. J-reduced energies $E_{red} = E_v(J,k,l) - B_0J(J+1) + D_J^0J^2(J+1)^2 - H_J^0J^3(J+1)^3$ around the 'Fermi' crossings of the $v_2 = v_3 = 1$ (red circle) and $v_6 = 2$, $l_6 = 0$ (blue diamond) levels, for $CH_3{}^{79}Br$. The values of J between which the crossings occur are indicated. (For interpretation of the references to colour in this figure legend, the reader is referred to the web version of this article.)

3.3. The $2\nu_6^0$ band

The authors of Ref. [8] assigned only four K-subbands ($K = 0$–3) of this weak parallel band. Following Ref. [8], these K-subbands seem unperturbed, even though an anharmonic interaction with $\nu_2 + \nu_3$ had already to be taken into account, in order to get more reasonable values for the B and D_{JK} rotational constants of this latter band. The best standard deviation of the least-squares fit of more than 700 lines of $\nu_2 + \nu_3$ was obtained in Ref. [8] using a coupling parameter $W_F = 1.82$ cm^{-1}; the centrifugal distortion parameters of $2\nu_6^0$ had to be constrained to the corresponding values of $2\nu_6^{\mp 2}$, because of the lack of information on the former band.

In the present study, a better knowledge of the band center of the $\nu_3 + \nu_5$ band allowed us to stabilize its Coriolis coupling with $\nu_2 + \nu_3$. The next step consisted in the refinement of the main anharmonic coupling parameter W_F. The obtained (preliminary) value, $W_F \sim 1.802$ cm^{-1}, allowed further achieving a better stability of the J-crossings, for several K values. In this way, we could easily assign a dozen of ${}^qR_9$ lines of $2\nu_6^0$, above $J = 36$ (Fig. 4), and find the corresponding ${}^qP_9$ lines by LSCD. We could finally show that the J value at which crossing occurs slightly depends on K. Crossing occurs at $J = 58$ for $K = 0$ and $K = 1$ levels, at $J = 57$ for $K = 2, \ldots$ and at $J = 36$ for $K = 9$ (Fig. 5). Situation is very similar for $CH_3{}^{81}Br$, with crossings occurring at slightly lower J values than for the ^{79}Br isotopologue. Finally, a total of 488 transitions of the $2\nu_6^0$ band were assigned for the ^{79}Br isotopologue, and 453 for the ^{81}Br one. Assignments span $K = 0$–10 for the former, and $K = 0$–12 for the latter.

4. Theoretical model

The general $\mathbf{H}_{mn}$ notation, where m is the total power of vibrational operators and n the total power of rotational operators, has been used throughout the paper, in the development of the rovibrational Hamiltonian. Such a term is of order $i = m + n - 2$ in the Amat and Nielsen classification [12].

The effective rovibrational Hamiltonian includes vibrational diagonal and off-diagonal contributions. The vibrational diagonal part, expanded up to fifth order, describes the individual vibrational states, i.e. the ground state, the $v_2 = v_3 = 1$ (A_1), $v_3 = v_5 = 1$ (E), and $v_6 = 2$ ($A_1 + E$) states. Several intra-vibrational interactions, such as q_{22} ($\Delta k = \Delta l = \pm 2$), q_{12} ($\Delta k = \pm 1$, $\Delta l = \mp 2$), f_{24} ($\Delta k = \pm 2$, $\Delta l = \mp 4$), and f_{44} ($\Delta k = \Delta l = \pm 4$) were also considered. The explicit forms of the corresponding matrix elements are given in Appendix A.

The vibrational off-diagonal part of the Hamiltonian contains all the relevant interactions coupling the studied vibrational levels, up to sixth order. This includes the Coriolis coupling ($\Delta k = \Delta l = \pm 1$) between $\nu_2 + \nu_3$ and $\nu_3 + \nu_5$, the anharmonic coupling ($\Delta k = \Delta l = 0$) between $\nu_2 + \nu_3$ and $2\nu_6^0$, but also a ($\Delta k = \pm 1$, $\Delta l = \mp 2$) interaction between $\nu_2 + \nu_3$ and $2\nu_6^{\mp 2}$, and finally a ($\Delta k = \pm 2$, $\Delta l = \mp 1$) interaction between $\nu_3 + \nu_5$ and $2\nu_6^0$. The corresponding matrix elements are listed in Appendix B.

5. Results and discussion

5.1. Reduction of the effective Hamiltonian for the $\nu_2 + \nu_3/\nu_3 + \nu_5$ Coriolis-interacting bands

The main 'global' rovibrational interaction affecting the studied levels is the x, y-Coriolis interaction, which couples the upper levels of the $\nu_2 + \nu_3$ and $\nu_3 + \nu_5$ bands. This interacting system is formally obtained by adding a quantum of the non-degenerate vibration ν_3 to the ν_2/ν_5 dyad. Hence, the reduction theory of the rovibrational Hamiltonian of ν_n/ν_t Coriolis-interacting bands in C_{3v} molecules, initiated by Lobodenko et al. [13] and developed

Table 2
Molecular parameters of $CH_3{}^{79}Br$ (in cm^{-1}) in the ground, $v_2 = v_3 = 1$, $v_3 = v_5 = 1$, and $v_6 = 2$ vibrational states.

$CH_3{}^{79}Br$	GS[a]	$v_2 = v_3 = 1$	$v_3 = v_5 = 1$	$v_6 = 2$, $l_6 = 0$	$v_6 = 2$, $l_6 = \mp 2$
E		1912.031799(54)	2051.149094(37)	1904.280328(54)	1912.719638(25)
B	0.319160556	0.31562950(22)	0.31662991(14)	0.316916685(78)	0.316864902(45)
A	5.180632	5.1947801(27)	5.1208536(36)	5.24066677(32)	5.2392929(14)
$D_J \times 10^7$	3.2932	3.3197(12)	3.37225(84)	3.32585(18)	3.32180(17)
$D_{JK} \times 10^6$	4.2913	4.2944(47)	5.0589(36)	4.3599(13)	4.3539(12)
$D_K \times 10^5$	8.47	8.7330(33)	8.0854(63)	9.1305(45)	9.1068(12)
$H_J \times 10^{13}$	−1.9	−1.9	−1.9	−1.9	−1.9
$H_{JK} \times 10^{12}$	3.2	3.2	3.2	3.2	3.2
$H_{KJ} \times 10^{10}$	1.97	1.97	1.97	1.97	1.97
$H_K \times 10^9$	4.1	4.1	4.1	4.1	4.1
$A\zeta$			−1.1369477(61)		1.1363355(17)
$\eta_J \times 10^5$			−1.6599(30)		0.99579(28)
$\eta_K \times 10^4$			−2.7506(34)		0.9787(11)
$\tau_{JK} \times 10^9$			2.96(71)		1.484 (77)
$\tau_K \times 10^8$			0.		−2.183(70)
$q_{12}^J \times 10^4$				4.821(26)	
$q_{22} \times 10^5$			0.	−7.3012(26)	
W_F				1.795308(78)	
$W_F^J \times 10^6$				7.0095	
$C_{11}^{(1)}$		0.194444(17)			
$C_{11}^{(3a)} \times 10^7$		−4.37(11)			
$C_{11}^{(2)} \times 10^3$		0.6731(18)			
$f_{41}^x \times 10^3$		−2.0791(58)			
$f_{43}^{xJ} \times 10^8$		−4.48(26)			
$f_{24} \times 10^7$					−9.79(22)
$f_{44} \times 10^9$					−2.2395(69)
$f_{42}^{xxa} \times 10^5$			−5.28(10)		
$f_{44}^{xxaJ} \times 10^8$			1.217(37)		
Number of IR data		855	640	488	1449
$\sigma \times 10^3$		0.286	0.463	0.332	0.288

Numbers in parentheses are standard deviations in units of the last digit quoted.
[a] Ref. [17].

further by Stříteská et al. [14], applies also to the $\nu_2 + \nu_3/\nu_3 + \nu_5$ system of CH_3Br. The authors of the latter paper pointed out that the most important 'transformed' interaction parameters, depending on two contact transformation parameters, s and s_1, are

$$\tilde{q}_{12} = q_{12} + \frac{1}{2}s(A - B + 2A\zeta)$$

$$\tilde{C}_{21}^{(2)} = C_{21}^{(2)} - sC_{11}^{(1)}$$

$$\tilde{q}_{22} = q_{22} - s_1 C_{11}^{(1)}$$

$$\tilde{C}_{11}^{(2)} = C_{11}^{(2)} - \frac{1}{2}s_1(A - B - A\zeta)$$

Hence, two out of the four above mentioned interaction parameters have to be fixed in order to determine the contact transformation parameters s and s_1.

In the present case, it has been found that the best reproduction of the experimental wavenumbers could be achieved by the refinement of the $C_{11}^{(2)}$ parameter, the q_{22} l-interaction parameter having been fixed to zero. In this case, the reduction theory [14] would require the refinement of q_{12} or $C_{21}^{(2)}$. However, neither of them could be significantly determined in the present work, which is probably due to the limited data set available for the $\nu_3 + \nu_5$ band. Finally, the interaction scheme for the $\nu_2 + \nu_3/\nu_3 + \nu_5$ system is very similar to the Model II employed by Kwabia Tchana et al. for the ν_2/ν_5 dyad [15]. Moreover, the $C_{11}^{(1)}$ and $C_{11}^{(2)}$ parameters obtained in the present work show a remarkable consistency with the corresponding values for the ν_2/ν_5 system.

5.2. Other vibrational and rovibrational interactions in the 2 $\nu_6/\nu_2 + \nu_3/\nu_3 + \nu_5$ band system

The other important interaction affecting the levels under consideration is the anharmonic resonance between $\nu_2 + \nu_3$ and $2\nu_6^0$. This interaction, already suggested in a theoretical paper [16], was also considered in the earlier experimental work of Najib et al. [8]. These latter authors obtained the best standard deviation of the fit ($0.0023\ cm^{-1}$) with a coupling parameter $W_F = 1.82\ cm^{-1}$ (held fixed) for both isotopologues. The present study allowed us to obtain values which are very close to the previous one. However, the main coupling parameter could be refined, thanks to the inclusion of several transitions below and above the crossings. We were even able to reveal a J-dependence of this anharmonic coupling; however, the corresponding coupling parameter (W_F^J) was held fixed for the $CH_3{}^{79}Br$ isotopologue in the final stage of our calculations. For the $CH_3{}^{81}Br$ isotopologue, the J-dependence of the anharmonic coupling seems to be slightly more pronounced and the corresponding parameter could be refined without significant worsening of the band centers accuracy for the $\nu_2 + \nu_3$ and $2\nu_6^0$ bands.

Another interaction, which has been thought as 'local' and hence of minor importance in Ref. [8], is that between the ($v_2 = v_3 = 1$, J, k) and ($v_6 = 2$, $l_6 = 2$, J, $k - 1$) levels. This interaction is indeed local, crossing occurring for only one couple of levels, ($v_2 = v_3 = 1$, J, $k = 1$) and ($v_6 = 2$, $l_6 = 2$, J, $k = 0$), at $J' = 45$. For the next couple of levels, crossing would occur at $J > 75$, which is beyond the observed rovibrational transitions. Nevertheless, the inclusion of this ($\Delta k = \pm 1$, $\Delta l = \mp 2$) interaction, originating from a $\mathbf{H}_{41}$ Hamiltonian term (see Appendix B), further determines the correct relative positions of the ($v_2 = v_3 = 1$)/($v_6 = 2$, $l_6 = 2$)/($v_6 = 2$, $l_6 = 0$) levels and subsequently the J-values of the anharmonic crossings between ($v_2 = v_3 = 1$) and ($v_6 = 2$, $l_6 = 0$).

Table 3
Molecular parameters of $CH_3{}^{81}Br$ (in cm^{-1}) in the ground, $v_2 = v_3 = 1$, $v_3 = v_5 = 1$, and $v_6 = 2$ vibrational states.

$CH_3^{81}Br$	GS[a]	$v_2 = v_3 = 1$	$v_3 = v_5 = 1$	$v_6 = 2$, $l_6 = 0$	$v_6 = 2$, $l_6 = \mp 2$
E		1910.825778(84)	2049.947662(40)	1904.151941(91)	1912.595450(30)
B	0.317947638	0.31443638(26)	0.31543005(15)	0.31571287(10)	0.315661444(50)
A	5.180615	5.1948043(30)	5.1207075(40)	5.2405876(34)	5.2392624(25)
$D_J \times 10^7$	3.2694	3.2994(16)	3.34977(93)	3.30246(22)	3.29839(17)
$D_{JK} \times 10^6$	4.2640	4.2499(32)	5.0789(40)	4.3204(11)	4.3203(21)
$D_K \times 10^5$	8.48	8.7391(35)	8.0889(68)	9.0733(24)	9.1255(34)
$H_J \times 10^{13}$	−1.9	−1.9	−1.9	−1.9	−1.9
$H_{JK} \times 10^{12}$	4.7	4.7	4.7	4.7	4.7
$H_{KJ} \times 10^{10}$	1.95	1.95	1.95	1.95	1.95
$H_K \times 10^9$	4.6	4.6	4.6	4.6	4.6
$A\zeta$			−1.1357820(65)		1.1357300(20)
$\eta_J \times 10^5$			−1.7038(23)		0.99086(36)
$\eta_K \times 10^4$			−2.8215(35)		0.9774(13)
$\tau_{JK} \times 10^9$			13.86(72)		1.86(11)
$\tau_K \times 10^8$					−2.45(13)
$q_{12}^I \times 10^4$				4.566(54)	
$q_{22} \times 10^5$			0.	−7.2335(31)	
W_F				1.79025(15)	
$W_F^J \times 10^6$				9.157(84)	
$C_{11}^{(1)}$		0.193699(21)			
$C_{11}^{(3a)} \times 10^7$		−4.71(14)			
$C_{11}^{(2)} \times 10^3$		0.6718(12)			
$f_{41}^x \times 10^3$		−2.1217(85)			
$f_{43}^{xJ} \times 10^8$		−3.37(60)			
$f_{24} \times 10^7$					−9.77(21)
$f_{44} \times 10^9$					−2.202(13)
$f_{42}^{xxa} \times 10^5$			−1.609(20)		
$f_{44}^{xxaJ} \times 10^8$			1.107(31)		
Number of IR data		687	647	475	1127
$\sigma \times 10^3$		0.188	0.537	0.307	0.286

Numbers in parentheses are standard deviations in units of the last digit quoted.
[a] Ref. [17].

In the least-squares fit, the ground state parameters were kept fixed to the values obtained by Sakai and Katayama [17][3]. The resulting 'diagonal' parameters of the interacting levels, together with the intra- and inter-vibrational interaction parameters, are listed in Table 2 for $CH_3{}^{79}Br$, and in Table 3 for $CH_3{}^{81}Br$.

6. Conclusion

The present work represents the first global high-resolution analysis of the $v_2 + v_3/v_3 + v_5/2v_6$ band system of methyl bromide, near 2000 cm^{-1}. All the relevant Coriolis and anharmonic interactions which connect the studied rovibrational levels were considered in the model, allowing thus to treat a considerably extended data set of more than 3000 transitions, for both the ^{79}Br and ^{81}Br isotopologues. The reproduction of all experimental data is quantitative and results in very accurate molecular parameters.

The analysis of the $v_3 + v_5$ combination band, together with previous analyses of the v_3 [19] and v_5 [15] fundamental bands, provides the anharmonicity constants $x_{35} = -2.90073(7)\ cm^{-1}$ for $CH_3{}^{79}Br$ and $-2.90852(7)\ cm^{-1}$ for $CH_3{}^{81}Br$. The x_{35} value is thus in perfect agreement with the estimation performed by Anttila et al. [20], using the $v_3 + v_5 - v_3$ hot band. Besides, two other anharmonicity parameters could be obtained in this work, $x_{66} = -0.61786(4)/-0.61824(5)$ and $g_{66} = 2.10983(2)/2.11088(2)$ for $CH_3{}^{79}Br/CH_3{}^{81}Br$ respectively.

[3] We have to notice that ground state parameters of CH_3Br were recently obtained by Ramos and Drouin [18], thanks to accurate measurements of the submillimeter spectrum up to 1.2 THz. Nevertheless, as the axial ground state constants were determinable in the above mentioned study only thanks to inclusion of (older) infrared ground-state combination differences, we have preferred using values reported in Ref. [17]. A re-determination of all ground state parameters, including the axial ones, seems thus mandatory.

Acknowledgements

The authors would like to thank Dr. Petr Pracna (Prague), for letting them use his fitting program SIMFIT.

Appendix A. Definition of matrix elements of the vibrational diagonal blocks in the effective vibration-rotation Hamiltonian

The diagonal matrix elements up to fifth order were taken as

$$\begin{aligned} E_{vr}(J,k,l) &= E_v + B_v J(J+1) + (A_v - B_v)k^2 - D_J^v J^2(J+1)^2 \\ &\quad - D_{JK}^v J(J+1)k^2 - D_K^v k^4 + H_J^v J^3(J+1)^3 \\ &\quad + H_{JK}^v J^2(J+1)^2 k^2 + H_{KJ}^v J(J+1)k^4 + H_K^v k^6 \\ &\quad + \left[-2A\zeta_v + \eta_J^v J(J+1) + \eta_K^v k^2 + \tau_J^v J^2(J+1)^2 \right. \\ &\quad \left. + \tau_{JK}^v J(J+1)k^2 + \tau_K^v k^4\right] kl \end{aligned} \tag{A1}$$

The z-Coriolis part vanishes for the non-degenerate vibrational levels, i.e. the ground, ($v_2 = v_3 = 1$) and ($v_6 = 2^0$) states.

In the $v_3 = v_5 = 1$ and the ($v_6 = 2$) levels, the following l-type operators have been used

$$\begin{aligned} &\langle v_t^{l_t \pm 2}; J, k \pm 2 \,|\mathbf{H}_{22} + \mathbf{H}_{24}|\, v_t^{l_t}; J, k\rangle \\ &= \left[(v_t \mp l_t)\,(v_t \pm l_t + 2)\right]^{1/2} \left\{ q_{22} + f_{22}^J J(J+1) \right. \\ &\quad \left. + f_{22}^K \left[k^2 + (k \pm 2)^2 \right] \right\} F_2^{\pm}(J,k) \end{aligned} \tag{A2}$$

$$\begin{aligned} &\langle v_t^{l_t \pm 2}; J, k \mp 1 | \mathbf{H}_{22} + \mathbf{H}_{24} | v_t^{l_t}; J, k\rangle \\ &= \left[(v_t \mp l_t)(v_t \pm l_t + 2)\right]^{1/2} \left\{ \left[q_{12} + f_{12}^J J(J+1) \right] (2k \mp 1) \right. \\ &\quad \left. + f_{12}^K \left[k^3 + (k \mp 1)^3 \right] \right\} F_1^{\mp}(J,k) \end{aligned} \tag{A3}$$

$$\langle v_t^{l_t\pm2};J,k\mp1|\mathbf{H}_{41}+\mathbf{H}_{43}|v_t^{l_t};J,k\rangle = [(v_t\mp l_t)(v_t\pm l_t+2)]^{1/2}\Big\{q_{12}^{l}+f_{12}^{ll}J(J+1)+f_{12}^{lK}\left[k^2+(k\mp1)^2\right]\Big\}2l_t\pm2\Big)F_1^{\mp}(J,k) \quad (A4)$$

$$\langle v_t^{l_t\pm4};J,k\mp2|\mathbf{H}_{42}|v_t^{l_t};J,k\rangle = \frac{1}{4}f_{24}\sqrt{(v_t\mp l_t-2)(v_t\mp l_t)(v_t\pm l_t+2)(v_t\pm l_t+4)}F_2^{\mp}(J,k) \quad (A5)$$

$$\langle v_t^{l_t\pm4};J,k\pm4|\mathbf{H}_{44}|v_t^{l_t};J,k\rangle = \frac{1}{4}f_{44}\sqrt{(v_t\mp l_t-2)(v_t\mp l_t)(v_t\pm l_t+2)(v_t\pm l_t+4)}F_4^{\pm}(J,k) \quad (A6)$$

The notation of the matrix elements of rotational shifting operators was taken conventionally as

$$F_n^{\pm}(J,k)=\prod_{i=1}^{n}[J(J+1)-(k\pm i\mp1)(k\pm i)]^{1/2} \quad (A7)$$

Appendix B. Definition of matrix elements of the interaction block in the effective vibration-rotation Hamiltonian

(1) Anharmonic interaction ($v_2 = v_3 = 1$)/($v_6 = 2^0$)

$$\left\langle 110^00^0;J,k\middle|\mathbf{H}_{40}+\mathbf{H}_{42}\middle|000^02^0;J,k\right\rangle = W_F+W_F^JJ(J+1)+W_F^Kk^2 \quad (B1)$$

(2) Rovibrational interactions

Coriolis and α-interactions, which are analogous to those used in the $v_2 = 1/v_5 = 1$ level system, were considered in the following form

$$\left\langle 110^00^0;J,k\middle|\mathbf{H}_{21}+\mathbf{H}_{23}\middle|011^{\pm1}0^0;J,k\pm1\right\rangle = \pm\sqrt{2}\Big\{C_{11}^{(1)}+C_{11}^{(3a)}J(J+1)+C_{11}^{(3b)}\left[k^2+(k\pm1)^2\right]\Big\}F_1^{\pm}(J,k) \quad (B2)$$

$$\left\langle 110^00^0;J,k\middle|\mathbf{H}_{22}\middle|011^{\pm1}0^0;J,k\pm1\right\rangle = \sqrt{2}C_{11}^{(2)}(2k\pm1)F_1^{\pm}(J,k) \quad (B3)$$

$$\left\langle 110^00^0;J,k\middle|\mathbf{H}_{22}\middle|011^{\pm1}0^0;J,k\mp2\right\rangle = \sqrt{2}C_{21}^{(2)}F_2^{\mp}(J,k) \quad (B4)$$

The ($\Delta k = \pm1$, $\Delta l = \mp2$) interaction between the ($v_2 = v_3 = 1$) and ($v_6 = 2$) levels has the following matrix elements

$$\left\langle 110^00^0;J,k\middle|\mathbf{H}_{41}^{x}\middle|000^02^{\pm2};J,k\mp1\right\rangle = \pm2\sqrt{2}f_{41}^{x}F_1^{\mp}(J,k) \quad (B5)$$

The ($\Delta k = \pm 2$, $\Delta l = \mp1$) interaction between the ($v_3 = v_5 = 1$) and ($v_6 = 2$) levels has the following matrix elements

$$\left\langle 000^02^0;J,k\mp2\middle|\mathbf{H}_{42}^{xxa}\middle|011^{\mp1}0^0;J,k\right\rangle = \sqrt{2}f_{42}^{xxa}F_2^{\mp}(J,k) \quad (B6)$$

$$\left\langle 000^02^{\pm2};J,k\mp2\middle|\mathbf{H}_{42}^{xxa}\middle|011^{\pm1}0^0;J,k\right\rangle = 2f_{42}^{xxb}F_2^{\mp}(J,k) \quad (B7)$$

Appendix C. Supplementary material

Supplementary data for this article are available on ScienceDirect (www.sciencedirect.com), as part of the Ohio State University Molecular Spectroscopy Archives (http://msa.lib.ohiostate.edu/jmsa_hp.htm).

Supplementary data associated with this article can be found, in the online version, at http://dx.doi.org/10.1016/j.jms.2017.05.010.

References

[1] S.A. Yvon-Lewis, E.S. Satzman, S.A. Montzka, Atmos. Chem. Phys. 9 (2009) 5963–5974.
[2] WMO (World Meteorological Organization), Scientific Assessment of Ozone Depletion: 2010, Global Ozone Research and Monitoring Project – Report No. 52, 516 pp., Geneva, Switzerland, 2011.
[3] Encyclopedia of Atmospheric Sciences (Second Edition), edited by Gerald R. North (Editor-in-Chief), John Pyle and Fuqing Zhang, Vol. 5, p. 228 (S. Yvon-Lewis and J. H. Butler), doi: http://dx.doi.org/10.1016/B978-0-12-382225-3.00467-9.
[4] N. Jacquinet-Husson et al., The 2015 edition of the GEISA spectroscopic database, J. Mol. Spectrosc. 327 (2016) (2015) 31–72.
[5] L.S. Rothman et al., The HITRAN 2012 molecular spectroscopic database, J. Quant. Spectrosc. Rad. Trans. 130 (2013) (2012) 4–50.
[6] C. Betrencourt-Stirnemann, G. Graner, D.E. Jennings, W.E. Blass, J. Mol. Spectrosc. 69 (1978) 179–198.
[7] Y. Morino, J. Nakamura, S. Yamamoto, Bull. Chem. Soc. Japan 38 (1965) 459–468.
[8] H. Najib, N. Bensari-Zizi, G. Guelachvili, C. Alamichel, J. Mol. Spectrosc. 114 (1985) 321–335.
[9] M. Ouahman, N. Bensari-Zizi, G. Guelachvili, C. Alamichel, J. Mol. Spectrosc. 129 (1988) 276–283.
[10] J.S. Garing, H.H. Nielsen, K. Narahari Rao, J. Mol. Spectrosc. 3 (1959) 496–527.
[11] W. Lodyga, M. Kreglewski, P. Pracna, Š. Urban, J. Mol. Spectrosc. 243 (2007) 182–188, http://dx.doi.org/10.1016/j.jms.2007.02.004.
[12] G. Amat, H.H. Nielsen, J. Chem. Phys. 36 (1962) 1859–1865.
[13] E.I. Lobodenko, O.N. Sulakshina, V.I. Perevalov, Vl.G. Tyuterev, J. Mol. Spectrosc. 126 (1987) 159–170.
[14] L. Nová Stříteská, K. SarkaŠ., Š. Urban, J. Mol. Spectrosc. 256 (2009) 135–140.
[15] F. Kwabia Tchana, I. Kleiner, J. Orphal, N. Lacome, O. Bouba, J. Mol. Spectrosc. 228 (2004) 441–452.
[16] S. Kondo, Y. Koga, T. Nakanaga, S. Saëki, J. Mol. Spectrosc. 100 (1983) 332–342.
[17] J. Sakai, M. Katayama, J. Mol. Struct. 190 (1988) 113–123.
[18] M. Ramos, B.J. Drouin, J. Mol. Spectrosc. 269 (2011) 187–192.
[19] R. Lakanen, M. Koivusaari, V.-M. Horneman, J. Kauppinen, J. Mol. Spectrosc. 135 (1989) 188–190.
[20] R. Anttila, C. Betrencourt-Stirnemann, J. Dupré, J. Mol. Spectrosc. 100 (1983) 54–74.